

Spherical Wavefront Near-Field DoA Estimation in THz Automotive Radar

Ahmet M. Elbir¹, Kumar Vijay Mishra^{1,2} and Symeon Chatzinotas¹

¹University of Luxembourg, Luxembourg

²United States DEVCOM Army Research Laboratory, Adelphi, MD 20783 USA

E-mail: ahmetmelbir@ieee.org, kvm@ieee.org, symeon.chatzinotas@uni.lu

Abstract—Automotive radar at terahertz (THz) band has the potential to provide compact design. The availability of wide bandwidth at THz-band leads to high range resolution. Further, very narrow beamwidth arising from large arrays yields high angular resolution up to milli-degree level direction-of-arrival (DoA) estimation. At THz frequencies and extremely large arrays, the signal wavefront is spherical in the near-field that renders traditional far-field DoA estimation techniques unusable. In this work, we examine near-field DoA estimation for THz automotive radar. We propose an algorithm using multiple signal classification (MUSIC) to estimate target DoAs and ranges while also taking beam-squint in near-field into account. Using an array transformation approach, we compensate for near-field beam-squint in noise subspace computations to construct the beam-squint-free MUSIC spectra. Numerical experiments show the effectiveness of the proposed method to accurately estimate the target parameters.

Index Terms—Automotive radar, DoA estimation, THz band, beam-squint, vehicular communications.

I. INTRODUCTION

Terahertz (THz) band, spanning from 0.1 to 10 THz, has emerged as a promising frontier for the realization of significant advancements in sixth-generation (6G) wireless networks [1]. Apart from gains in the communications performance, THz-band is also currently investigated to ensure milli-degree precision in direction-of-arrival (DoA) estimation in THz automotive radar [2–4]. Other advantages of THz-band sensing include small form factor, wide bandwidth, and near-optical resolution [5–9].

High-resolution DoA estimation within the THz-band, however, is impeded by myriad challenges such as high path losses, molecular absorption, and intricate propagation/scattering dynamics [1, 10]. To compensate these losses, large number of antennas are employed to improve the beamforming gain [11]. Furthermore, hybrid analog/digital beamforming architectures with phase shifter networks are used to reduce the number of radio-frequency (RF) chains. THz systems also suffer from *beam-squint* arising from the subcarrier-independent analog beamformers [12–14]. This leads to misaligned beam generation at different subcarrier-squint in the spatial domain; that is, the main lobes of the array gain corresponding to the lowest and highest subcarriers do not overlap because of ultra-wide bandwidth (Fig. 1). This significantly degrades DoA estimation [4, 14].

Notably, existing countermeasures for beam-squint are predominantly hardware-based [15]. Here, additional hardware components such as time-delayer networks are realized to generate a negative group-delay for its compensation [13]. This approach is expensive because each phase shifter of the network is connected to multiple delayer elements, each of which consumes approximately 150% more power than a single phase shifter at THz band [4]. THz channel estimation [14] and hybrid analog/digital beamforming [7, 12, 13] under beam-squint have been explored in prior THz studies, which largely omit discussions on DoA estimation. While the DoA estimation problem is studied for both THz [2] and millimeter-wave [16, 17], the impact of beam-squint is generally excluded from such studies.

Besides beam-squint, another formidable challenge in THz-band signal processing is short-transmission distance. While some experiments indicate that a maximum range of 200 m is possible for THz automotive radars [18], practical operations are envisaged only in the 10-20 m range [5]. Together with high THz frequencies and usage of extremely large (XL) arrays, the received signal wavefront at close ranges is spherical in near-field (Fig. 2). In general, the wavefront is spherical in the near-field when the transmission range is shorter than the Fraunhofer distance [19, 20]. THz automotive radars must, therefore, accommodate the near-field beampattern for DoA estimation, which now depends on both direction and range information [4]. Among prior works, [8, 21–23] consider near-field processing for THz systems but ignore the effect of beam-squint. Range-dependent beampattern is also observed in some far-field applications such as frequency diverse array (FDA) radars [24, 25] and quantum Rydberg arrays [26, 27]. However, the wavefront is not spherical in these applications.

In this paper, we examine the near-field DoA estimation problem for THz automotive radar in the presence of beam-squint. We first present the near-field signal model as well as the beam-squint model. Then, a subarrayed approach is devised to collect and process the antenna array outputs for high resolution DoA estimation. We propose a modified *multiple signal classification* (MUSIC) algorithm [28] with noise subspace correction approach to account for the beam-squint and accurately estimate the targets. In order to obtain the corrected noise subspace, we introduce a linear transformation matrix that constructs a mapping the nominal and the beam-squint-distorted steering vectors in spherical wave domain,

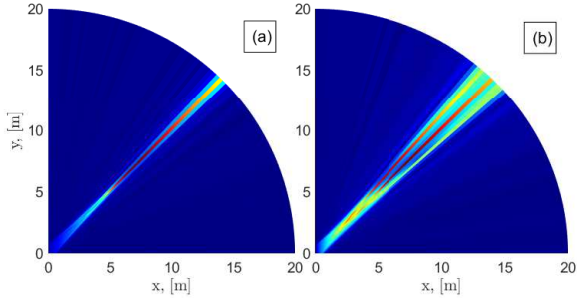


Fig. 1. Array gain of a single target at 45° and 10 m for (a) narrowband and (b) wideband scenario when $f_c = 300$ GHz, $B = 10$ MHz and $B = 30$ GHz, respectively.

which facilitates the rectification of the skewed noise-subspace matrix derived from the covariance of the array data. The performance of the proposed approach is evaluated via numerical experiments, and it can effectively estimate the target DoA angles and ranges in the presence of near-field beam-squint.

II. SYSTEM MODEL

Consider a wideband THz automotive radar system (Fig. 2) that comprises hybrid analog/digital beamformers performed over M subcarriers with N -element uniform linear array (ULA) and N_{RF} RF chains. The radar employs a subcarrier-independent precoder $\mathbf{F} \in \mathbb{C}^{N \times N_{\text{RF}}}$ to sense the environment. The sensing signal generated for the m -th subcarrier is $\mathbf{s}_m(t_i) \in \mathbb{C}^{N_{\text{RF}}}$, where $i = 1, \dots, T$, and T is the number of snapshots along the fast-time axis [29]. To sense the environment, N_{RF} RF chains are activated and the transmitted probing signal is

$$\mathbf{X}_m = [\mathbf{x}_m(t_1), \dots, \mathbf{x}_m(t_T)] \in \mathbb{C}^{N \times T}, \quad (1)$$

where $\mathbf{x}_m(t_i) = \mathbf{F}\mathbf{s}_m(t_i) \in \mathbb{C}^N$, $\mathbb{E}\{\mathbf{X}_m\mathbf{X}_m^H\} = \frac{P_r T}{MN} \mathbf{I}_N$, $\mathbf{F}\mathbf{F}^H = \mathbf{I}_N$, and P_r is the radar transmit power.

A. Near-field

The use of high THz frequencies and XL arrays implies that the short-range targets may lie in the near-field region, wherein the planar wave propagation does not hold. At ranges shorter than the Fraunhofer distance $d_F = \frac{2D^2}{\lambda}$, where D is the array aperture and $\lambda = \frac{c_0}{f_c}$ is the wavelength, the near-field wavefront is spherical [14, 19]. For a ULA, the array aperture is $D = (N-1)d$, where $d = \frac{\lambda}{2}$ is the element spacing. In the THz spectrum, it is imperative to employ a near-field signal model because $r_k < d_F$. For instance, when $f_c = 300$ GHz and $N = 256$, the Fraunhofer distance is $d_F = 32.76$ m.

Suppose that there are K targets at the physical locations $\{\theta_k, r_k\}_{k=1}^K$, where θ_k and r_k denote the DoA and the range of the k -th target. Taking into account the spherical-wave model [19, 30, 31], define the near-field steering vector

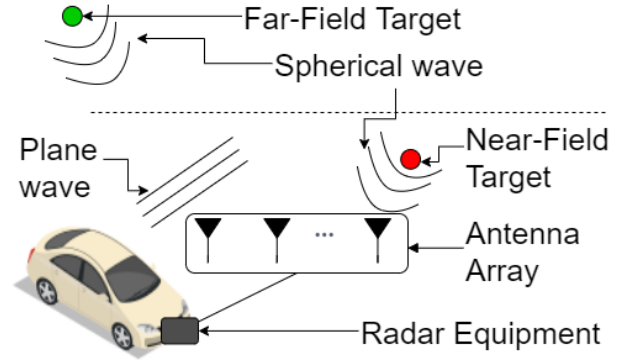


Fig. 2. An illustration of THz automotive radar and the received signal wavefronts from far- and near-field targets.

$\mathbf{a}(\theta_k, r_k) \in \mathbb{C}^N$ corresponding to the physical DoA θ_k and range r_k as

$$\mathbf{a}(\theta_k, r_k) = \frac{1}{\sqrt{N}} [e^{-j2\pi \frac{d}{\lambda} r_k^{(1)}}, \dots, e^{-j2\pi \frac{d}{\lambda} r_k^{(N)}}]^\top, \quad (2)$$

where $r_k^{(n)}$ is the distance between the k -th target and the n -th radar antenna, i.e.,

$$r_k^{(n)} = \sqrt{r_k^2 + 2(n-1)^2 d^2 - 2r_k(n-1)d\theta_k}. \quad (3)$$

Following the Fresnel approximation [30, 31], (3) becomes

$$r_k^{(n)} \approx r_k - (n-1)d\theta_k + (n-1)^2 d^2 \zeta_k, \quad (4)$$

where $\zeta_k = \frac{1-\theta_k^2}{2r_k}$. Rewrite (2) as

$$\mathbf{a}(\theta_k, r_k) \approx e^{-j2\pi \frac{f_c}{c_0} r_k} \tilde{\mathbf{a}}(\theta_k, r_k), \quad (5)$$

where the n -th element of $\tilde{\mathbf{a}}(\theta_k, r_k) \in \mathbb{C}^N$ is

$$[\tilde{\mathbf{a}}(\theta_k, r_k)]_n = e^{j2\pi \frac{f_c}{c_0} ((n-1)d\theta_k - (n-1)^2 d^2 \zeta_k)}. \quad (6)$$

B. Beam-squint

The steering vector in (5) corresponds to the physical location (θ_k, r_k) . Due to beam-squint, this deviates to the spatial location $(\bar{\theta}_{m,k}, \bar{r}_{m,k})$ in the beamspace because of the absence of subcarrier-dependent analog beamformers. Then, the n -th entry of the deviated steering vector in (6) for the spatial location is

$$[\tilde{\mathbf{a}}(\bar{\theta}_{m,k}, \bar{r}_{m,k})]_n = e^{j2\pi \frac{f_m}{c_0} ((n-1)d\bar{\theta}_{m,k} - (n-1)^2 d^2 \bar{\zeta}_{m,k})}. \quad (7)$$

Recall the following useful result to establish the relationship between the physical and spatial DoAs/ranges.

Proposition 1. [31] Denote $\mathbf{u} \in \mathbb{C}^N$ and $\mathbf{v}_m \in \mathbb{C}^N$ as the near-field steering vectors corresponding to the physical (i.e., $\{\theta_k, r_k\}$) and spatial (i.e., $\{\bar{\theta}_{m,k}, \bar{r}_{m,k}\}$) locations given in (6) and (7), respectively. Then, in spatial domain at subcarrier frequency f_m , the array gain achieved by $\mathbf{u}^H \mathbf{v}_m$ is maximized and the generated beam is focused at the location $\{\bar{\theta}_{m,k}, \bar{r}_{m,k}\}$

such that

$$\bar{\theta}_{m,k} = \eta_m \theta_k, \quad \bar{r}_{m,k} = \frac{1 - \eta_m^2 \theta_k^2}{\eta_m (1 - \theta_k^2)} r_k, \quad (8)$$

where $\eta_m = \frac{f_c}{f_m}$ represents the proportional deviation of DoA/ranges.

Following (4) and (8), define the near-field beam-squint in terms of DoAs and ranges as, respectively,

$$\Delta(\theta_k, m) = \bar{\theta}_{m,k} - \theta_k = (\eta_m - 1)\theta_k, \quad (9)$$

and

$$\begin{aligned} \Delta(r_k, m) &= \bar{r}_{m,k} - r_k = (\eta_m - 1)r_k \\ &= (\eta_m - 1) \frac{1 - \eta_m^2 \theta_k^2}{\eta_m (1 - \theta_k^2)} r_k. \end{aligned} \quad (10)$$

Define the received $N \times T$ target echo signal impinging on the antenna array at the m -th subcarrier as

$$\tilde{\mathbf{Y}}_m = \sum_{k=1}^K \mathbf{a}(\bar{\theta}_{m,k}, \bar{r}_{m,k}) \tilde{\mathbf{x}}_{m,k} + \tilde{\mathbf{N}}_m, \quad (11)$$

where $\tilde{\mathbf{N}}_m \sim \mathcal{CN}(\mathbf{0}, \sigma^2 \mathbf{I}_N)$ is temporarily and spatially white zero-mean complex Gaussian noise matrix of size $N \times T$ with variance σ^2 ; $\tilde{\mathbf{x}}_{m,k} \in \mathbb{C}^{1 \times T}$ denotes the echo signal reflected from the k -th target as $\tilde{\mathbf{x}}_{m,k} = \beta_{m,k} \mathbf{a}^\top(\bar{\theta}_{m,k}, \bar{r}_{m,k}) \mathbf{X}_m$; and $\beta_{m,k} \in \mathbb{C}$ is the reflection coefficient.

Our goal is to estimate the DoA and ranges of the targets, given that the array outputs from N antennas.

III. PROPOSED APPROACH

As $N_{\text{RF}} < N$, the size of the $N \times 1$ received signal in (11) is reduced to $N_{\text{RF}} \times 1$ after combining process as

$$\check{\mathbf{Y}}_m = \sum_{k=1}^K \check{\mathbf{W}}^H \mathbf{a}(\bar{\theta}_{m,k}, \bar{r}_{m,k}) \check{\mathbf{x}}_{k,m} + \check{\mathbf{W}}^H \tilde{\mathbf{N}}_m, \quad (12)$$

where $\check{\mathbf{W}} \in \mathbb{C}^{N \times N_{\text{RF}}}$ represents the analog combiner matrix.

A. Data Collection

To collect the full array data from N_{RF} RF chains, we follow a subarrayed approach. That is, the radar activates the antennas in a subarrayed fashion to obtain $N \times 1$ array data in $J = \frac{N}{N_{\text{RF}}}$ time slots. This is consistent with THz radar wherein the coherence time is of the order of picoseconds [2, 29]. Let $\mathbf{W}_j \in \mathbb{C}^{N \times N_{\text{RF}}}$ be the applied combiner matrix at the j -th time slot (instead of $\check{\mathbf{W}}$ in (12)) as $\mathbf{W}_j = \left[\mathbf{0}_{j N_{\text{RF}} \times N_{\text{RF}}}^\top, \bar{\mathbf{W}}_j^\top, \mathbf{0}_{N-(j+1) N_{\text{RF}} \times N_{\text{RF}}}^\top \right]^\top \in \mathbb{C}^{N \times N_{\text{RF}}}$, where $\bar{\mathbf{W}}_j \in \mathbb{C}^{N_{\text{RF}} \times N_{\text{RF}}}$ represents the combiner for the j -th block for $j = 1, \dots, J$. Then, the $N_{\text{RF}} \times T$ echo signal reflected from K targets at the j -th time slot is

$$\begin{aligned} \mathbf{Y}_{j,m} &= \sum_{k=1}^K \mathbf{W}_j^H \mathbf{a}(\bar{\theta}_{m,k}, \bar{r}_{m,k}) \tilde{\mathbf{x}}_{m,k} + \mathbf{W}_j^H \tilde{\mathbf{N}}_m \\ &= \sum_{k=1}^K \beta_{m,k} \mathbf{W}_j^H \mathbf{a}_{m,k} \mathbf{a}_{m,k}^\top \mathbf{X}_m + \mathbf{N}_{j,m}, \end{aligned} \quad (13)$$

where $\mathbf{a}_{m,k} = \mathbf{a}(\bar{\theta}_{m,k}, \bar{r}_{m,k}) \in \mathbb{C}^N$ and $\mathbf{N}_{j,m} = \mathbf{W}_j^H \tilde{\mathbf{N}}_m \in \mathbb{C}^{N_{\text{RF}} \times T}$ represents the noise term. Define

$$\mathbf{A}_m = [\mathbf{a}_{m,1}, \dots, \mathbf{a}_{m,K}] \in \mathbb{C}^{N \times K}, \quad (14)$$

$$\mathbf{D}_{j,m} = \mathbf{W}_j^H \mathbf{A}_m \in \mathbb{C}^{N_{\text{RF}} \times K}, \quad (15)$$

$$\mathbf{\Pi}_m = \text{diag}\{\beta_{m,1}, \dots, \beta_{m,K}\} \in \mathbb{C}^{K \times K}, \quad (16)$$

Then, (13) becomes

$$\mathbf{Y}_{j,m} = \mathbf{D}_{j,m} \mathbf{\Pi}_m \mathbf{A}_m^\top \mathbf{X}_m + \mathbf{N}_{j,m}. \quad (17)$$

Stacking all $\mathbf{Y}_{j,m}$ into a single $N \times T$ matrix leads to the overall observation matrix $\mathbf{Y}_m \in \mathbb{C}^{N \times T}$ as $\mathbf{Y}_m = [\mathbf{Y}_{1,m}^\top, \dots, \mathbf{Y}_{J,m}^\top]^\top$, i.e.,

$$\mathbf{Y}_m = \mathbf{D}_m \mathbf{\Pi}_m \mathbf{A}_m^\top \mathbf{X}_m + \mathbf{N}_m, \quad (18)$$

where $\mathbf{D}_m = [\mathbf{D}_{1,m}^\top, \dots, \mathbf{D}_{J,m}^\top]^\top = \mathbf{W}^H \mathbf{A}_m \in \mathbb{C}^{N \times K}$, $\mathbf{W} = [\mathbf{W}_1, \dots, \mathbf{W}_J] \in \mathbb{C}^{N \times N}$ and $\mathbf{N}_m = [\mathbf{N}_{1,m}^\top, \dots, \mathbf{N}_{J,m}^\top]^\top$. The $N \times T$ array output data in (18) is collected via limited number of RF chains from multiple time slots. This is used to construct the covariance matrix to invoke the MUSIC algorithm.

B. Parameter Estimation

Next, we introduce the corrected noise subspace for beam-squint to accurately estimate the physical DoA and ranges. Define the $N \times N$ covariance matrix of the observations in (18) as $\mathbf{R}_m = \frac{1}{T} \mathbf{Y}_m \mathbf{Y}_m^H$, i.e.,

$$\begin{aligned} \mathbf{R}_m &= \frac{1}{T} \mathbf{D}_m \left(\frac{P_r T}{MN} \tilde{\mathbf{\Pi}}_m \right) \mathbf{D}_m^H + \frac{1}{T} \mathbf{N}_m \mathbf{N}_m^H \\ &\approx \frac{P_r}{MN} \mathbf{D}_m \tilde{\mathbf{\Pi}}_m \mathbf{D}_m^H + \frac{\sigma^2}{N} \mathbf{I}_N, \end{aligned} \quad (19)$$

where $\mathbf{N}_m \mathbf{N}_m^H \approx \frac{\sigma^2 T}{N} \mathbf{I}_N$ (because $\mathbf{W}^H \mathbf{W} = \frac{1}{N}$) and

$$\tilde{\mathbf{\Pi}}_m = \mathbf{\Pi}_m \mathbf{A}_m^\top \mathbf{A}_m^* \mathbf{\Pi}_m^H \in \mathbb{C}^{K \times K}. \quad (20)$$

The eigendecomposition of \mathbf{R}_m yields $\mathbf{R}_m = \mathbf{U}_m \mathbf{\Sigma}_m \mathbf{U}_m^H$, where $\mathbf{\Sigma}_m \in \mathbb{C}^{N \times N}$ is a diagonal matrix composed of the eigenvalues of \mathbf{R}_m in a descending order; $\mathbf{U}_m = [\mathbf{U}_m^S, \mathbf{U}_m^N] \in \mathbb{C}^{N \times N}$ corresponds to the eigenvector matrix; $\mathbf{U}_m^S \in \mathbb{C}^{N \times K}$ and $\mathbf{U}_m^N \in \mathbb{C}^{N \times N-K}$ are the signal and noise subspace eigenvector matrices, respectively.

By exploiting the orthogonality of the signal and noise subspaces, i.e., $\mathbf{U}_m^N \perp \mathbf{U}_m^S$, and the fact that the columns of \mathbf{U}_m^S and \mathbf{D}_m span the same subspace [28, 32], we have

$$\|\mathbf{d}_{m,k}^H \mathbf{U}_m^N\|_2^2 = 0, \quad (21)$$

where $\mathbf{d}_{m,k} = \mathbf{W}^H \mathbf{a}(\bar{\theta}_{m,k}, \bar{r}_{m,k}) \in \mathbb{C}^N$ is the k -th column of $\mathbf{D}_m \in \mathbb{C}^{N \times K}$.

Note that (21) implies the orthogonality with the corrupted steering vector $\mathbf{d}_{m,k}$, whereas our aim is to estimate the beam-squint-free physical DOA/ranges θ_k, r_k . Therefore, define $\mathbf{V}_m^N \in \mathbb{C}^{N \times N-K}$ as the beam-squint-corrected noise subspace matrix, which is orthogonal to the nominal steering vectors. To that end, denote the beam-squint transformation matrix by

$\mathbf{T}_m(\theta_k, r_k) \in \mathbb{C}^{N \times N}$. This provides a linear mapping between the nominal and beam-squint-corrupted steering vectors as

$$\mathbf{a}(\bar{\theta}_{m,k}, \bar{r}_{m,k}) = \mathbf{T}_m(\theta_k, r_k) \mathbf{a}(\theta_k, r_k), \quad (22)$$

where $\mathbf{T}_m(\theta_k, r_k) = \text{diag}\{\boldsymbol{\tau}_m(\theta_k, r_k)\}$, for which the n -th element of $\boldsymbol{\tau}_m(\theta_k, r_k) \in \mathbb{C}^N$ is $\tau_{m,k,n} = [\mathbf{a}(\bar{\theta}_{m,k}, \bar{r}_{m,k})]_n / [\mathbf{a}(\theta_k, r_k)]_n$. Using (22), (21) becomes

$$\begin{aligned} & \left\| \left(\mathbf{W}^H \mathbf{a}(\bar{\theta}_{m,k}, \bar{r}_{m,k}) \right)^H \mathbf{U}_m^N \right\|_2^2 \\ &= \left\| \mathbf{a}^H(\theta_k, r_k) \mathbf{T}_m^H(\theta_k, r_k) \mathbf{W} \mathbf{U}_m^N \right\|_2^2 \\ &= \left\| \mathbf{a}^H(\theta_k, r_k) \mathbf{V}_m^N \right\|_2^2 = 0, \end{aligned} \quad (23)$$

where \mathbf{V}_m^N is the corrected noise subspace matrix, i.e.,

$$\mathbf{V}_m^N \triangleq \mathbf{T}_{m,k}^H \mathbf{G}_m^H \mathbf{W} \mathbf{U}_m^N. \quad (24)$$

Examining (23) reveals the useful property regarding the orthogonality of the corrected noise subspace \mathbf{V}_m^N and the beam-squint-free steering vectors as $\mathbf{a}(\theta_k, r_k) \perp \mathbf{V}_m^N$ for $m \in \mathcal{M}$. Consequently, we write the beam-squint-corrected MUSIC spectra for M subcarriers as

$$P(\theta, r) = \sum_{m=1}^M \frac{1}{\mathbf{a}^H(\theta, r) \mathbf{V}_m^N \mathbf{V}_m^{N H} \mathbf{a}(\theta, r)}, \quad (25)$$

whose K highest peaks correspond to the physical target DoAs/ranges $\{\hat{\theta}_k, \hat{r}_k\}_{k=1}^K$, which can be identified through a peak-finding algorithm for (25) only once because it includes the combination of spectra for M subcarriers.

Algorithm 1 Near-field MUSIC

- Input:** $\mathbf{Y}_m, \mathbf{W}, K, \Psi, \mathcal{R}, \eta_m$ for $m \in \mathcal{M}$.
Output: $\{\hat{\theta}_k, \hat{r}_k\}_{k=1}^K$.
1: $\mathbf{R}_m = \frac{1}{T} \mathbf{Y}_m \mathbf{Y}_m^H$ for $m \in \mathcal{M}$.
2: Obtain the noise subspace \mathbf{U}_m^N from \mathbf{R}_m for $m \in \mathcal{M}$.
3: **for** $\theta \in \Psi$ and $r \in \mathcal{R}$ **do**
4: **for** $m \in \mathcal{M}$
5: Construct $\mathbf{a}(\theta, r)$ and $\mathbf{a}(\bar{\theta}_m, \bar{r}_m)$ from (6) and (7).
6: Construct $\mathbf{T}_m(\theta, r)$ as in (22).
7: $\mathbf{V}_m^N \leftarrow \mathbf{T}_m^H(\theta, r) \mathbf{W} \mathbf{U}_m^N$.
8: $P_m(\theta, r) \leftarrow \frac{1}{\mathbf{a}^H(\theta, r) \mathbf{V}_m^N \mathbf{V}_m^{N H} \mathbf{a}(\theta, r)}$.
9: **end for**
10: **end for**
11: Combined MUSIC spectra: $P(\theta, r) \leftarrow \sum_{m=1}^M P_m(\theta, r)$.
12: Find $\{\hat{\theta}_k, \hat{r}_k\}_{k=1}^K$ from the K highest peaks of $P(\theta, r)$.
-

Algorithm 1 presents the algorithmic steps for the proposed approach. Specifically, we first compute the beam-squint-corrupted noise subspace \mathbf{U}_m^N and the beam-squint transformation matrix $\mathbf{T}_m(\theta, r)$ for $\theta \in \Psi = [-1, 1]$ and $r \in \mathcal{R} = [0, d_F]$ in Steps 2-5. By constructing the corrected noise subspace \mathbf{V}_m^N in Step 7, the two-dimensional (2-D) MUSIC spectra $P_m(\theta, r)$ is computed in Step 8 for the m -th subcarrier. Then, the estimated DoA angles and ranges $\hat{\theta}_k, \hat{r}_k$ are computed from the combined 2-D MUSIC spectra $P(\theta, r)$ in Step 11.

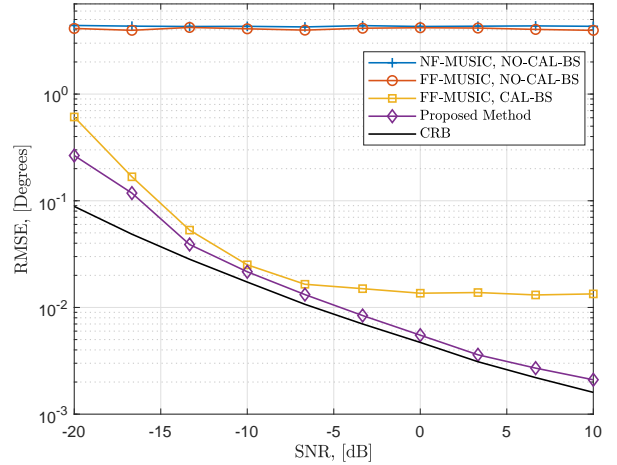


Fig. 3. DoA estimation RMSE vs. SNR.

C. Computational Complexity and Identifiability

The complexity of the proposed approach is mainly due to eigendecomposition of \mathbf{R}_m ($O(MN^3)$) as well as the computation the corrected noise subspace \mathbf{V}_m^N ($O(MN^2[3N - K])$) for $m \in \mathcal{M}$. Thus, the overall computational complexity order is $O(MN^2[4N - K])$. Note that the complexity reduces to $O(2MN^3)$ for the traditional MUSIC algorithm, which does not account for beam-squint. The problem of target localization involves K coupled (DoA and range) unknowns, while the collected array data from N_{RF} RF chains for $J = \frac{N}{N_{\text{RF}}}$ time-slots is $N \times 1$ for M subcarriers. Hence, the proposed technique is feasible only if $\text{rank}\{\mathbf{U}_m^N \mathbf{U}_m^{N H}\} = N - K \geq 1$, provided that $T \geq K$ data snapshots are available. This condition becomes $N_{\text{RF}} - K \geq 1$ if the output for a single time-slot is used.

IV. NUMERICAL EXPERIMENTS

The efficiency of our proposed method is benchmarked against the far-field and near-field MUSIC algorithms and beam-squint-corrected MUSIC algorithm as well as the Cramér-Rao bound (CRB) [14] in terms of root-MSE (RMSE), i.e., $\text{RMSE}_\theta = \left(\frac{1}{J_T K} \sum_{i=1}^{J_T} \sum_{k=1}^K |\hat{\theta}_{i,k} - \theta_{i,k}|^2 \right)^{1/2}$ and $\text{RMSE}_r = \left(\frac{1}{J_T K} \sum_{i=1}^{J_T} \sum_{k=1}^K |\hat{r}_{i,k} - r_{i,k}|^2 \right)^{1/2}$, where $\hat{\theta}_{i,k}$ and $\hat{r}_{i,k}$ stand for the estimated DoA and the ranges, respectively, for the i -th instance of $J_T = 500$ Monte Carlo trials. The default simulation parameters are $f_c = 300$ GHz, $B = 30$ GHz, $M = 32$, $N = 128$, $N_{\text{RF}} = 8$, $T = 500$, $K = 2$ [2, 12]. The DoAs are selected uniform at random from the interval $\hat{\theta}_k \sim \text{unif}[-\frac{\pi}{2}, \frac{\pi}{2}]$. The combiner matrix is modeled as $[\mathbf{W}]_{i,j} = \frac{1}{\sqrt{N}} e^{j\Phi}$, where $\Phi \sim \text{unif}[-\frac{\pi}{2}, \frac{\pi}{2}]$ for $i \in [1, N]$ and $j \in [1, N_{\text{RF}}]$.

Fig. 3 shows the DoA estimation RMSE with respect to signal-to-noise ratio (SNR), defined as $\text{SNR} = 10 \log_{10}(\frac{\rho}{\sigma_n^2})$ with $\rho = \frac{P_r}{M^2 N^2} = 1$. We see that both near-field (NF) and far-field (FF) MUSIC algorithms display poor performance (\sim

4°) without beam-squint calibration (NO-CAL-BS) whereas FF-MUSIC achieves relatively lower DoA estimation RMSE ($\sim 0.015^\circ$) when beam-squint is perfectly calibrated (CAL-BS). This observation shows that the impact of beam-squint is more severe than the near/far-field model mismatch. While the a priori calibration of beam-squint significantly reduces the DoA estimation RMSE, the proposed approach outperforms the competing algorithms by attaining the CRB very closely. This superior performance of the proposed approach can be attributed to the calibration of near-field beam-squint without any priori knowledge, thereby proving high resolution DoA accuracy.

V. SUMMARY

We investigated the near-field DoA estimation problem for THz automotive radar. We propose a MUSIC-like approach with noise subspace correction in order to compensate for the beam-squint. The performance of the proposed method is evaluated in the presence of near-field beam-squint. It is shown that the DoA error due to beam-squint is more severe ($\sim 4^\circ$) than that of near/far model mismatch ($\sim 0.01^\circ$). In contrast, our proposed method exhibits accurate DoA estimation performance with high precision.

REFERENCES

- [1] I. F. Akyildiz, C. Han, Z. Hu, S. Nie, and J. M. Jornet, "Terahertz Band Communication: An Old Problem Revisited and Research Directions for the Next Decade," *IEEE Trans. Commun.*, vol. 70, no. 6, pp. 4250–4285, May 2022.
- [2] Y. Chen, L. Yan, C. Han, and M. Tao, "Millidegree-Level Direction-of-Arrival Estimation and Tracking for Terahertz Ultra-Massive MIMO Systems," *IEEE Trans. Wireless Commun.*, vol. 21, no. 2, pp. 869–883, Aug. 2021.
- [3] B. Peng and T. Kürner, "Three-Dimensional Angle of Arrival Estimation in Dynamic Indoor Terahertz Channels Using a Forward-Backward Algorithm," *IEEE Trans. Veh. Technol.*, vol. 66, no. 5, pp. 3798–3811, Aug. 2016.
- [4] A. M. Elbir, K. V. Mishra, S. Chatzinotas, and M. Bennis, "Terahertz-Band Integrated Sensing and Communications: Challenges and Opportunities," *arXiv*, Aug. 2022.
- [5] S. Bhattacharjee, K. V. Mishra, R. Annavaajala, and C. R. Murthy, "Multi-Carrier Wideband OCDM-Based THz Automotive Radar," in *ICASSP 2023 - 2023 IEEE International Conference on Acoustics, Speech and Signal Processing (ICASSP)*. IEEE, pp. 04–10.
- [6] Y. Xiao, F. Norouzian, E. G. Hoare, E. Marchetti, M. Gashinova, and M. Cherniakov, "Modeling and Experiment Verification of Transmissivity of Low-THz Radar Signal Through Vehicle Infrastructure," *IEEE Sens. J.*, vol. 20, no. 15, pp. 8483–8496, Mar. 2020.
- [7] A. M. Elbir, K. V. Mishra, and S. Chatzinotas, "Terahertz-Band Joint Ultra-Massive MIMO Radar-Communications: Model-Based and Model-Free Hybrid Beamforming," *IEEE J. Sel. Top. Signal Process.*, vol. 15, no. 6, pp. 1468–1483, Oct. 2021.
- [8] A. Eamaz, F. Yeganegi, K. V. Mishra, and M. Soltanalian, "Near-field low-WISL unimodular waveform design for terahertz automotive radar," in *European Signal Processing Conference*, 2023, pp. 1–5.
- [9] K. V. Mishra, I. Bilik, J. Tabrikian, and A. P. Petropulu, "Signal processing for terahertz-band automotive radars: Exploring the next frontier," *arXiv preprint*, 2023.
- [10] H. Sariyedeen, M.-S. Alouini, and T. Y. Al-Naffouri, "An overview of signal processing techniques for Terahertz communications," *Proceedings of the IEEE*, vol. 109, no. 10, pp. 1628–1665, 2021.
- [11] A. M. Elbir, K. V. Mishra, S. A. Vorobyov, and R. W. Heath, "Twenty-Five Years of Advances in Beamforming: From convex and nonconvex optimization to learning techniques," *IEEE Signal Process. Mag.*, vol. 40, no. 4, pp. 118–131, Jun. 2023.
- [12] L. Dai, J. Tan, Z. Chen, and H. V. Poor, "Delay-Phase Precoding for Wideband THz Massive MIMO," *IEEE Trans. Wireless Commun.*, p. 1, Mar. 2022.
- [13] B. Wang, M. Jian, F. Gao, G. Y. Li, and H. Lin, "Beam Squint and Channel Estimation for Wideband mmWave Massive MIMO-OFDM Systems," *IEEE Trans. Signal Process.*, vol. 67, no. 23, pp. 5893–5908, Oct. 2019.
- [14] A. M. Elbir, W. Shi, A. K. Papazafireopoulos, P. Kourtessis, and S. Chatzinotas, "Terahertz-Band Channel and Beam Split Estimation via Array Perturbation Model," *IEEE Open J. Commun. Soc.*, p. 1, Mar. 2023.
- [15] J. Tan and L. Dai, "Wideband Beam Tracking in THz Massive MIMO Systems," *IEEE J. Sel. Areas Commun.*, vol. 39, no. 6, pp. 1693–1710, Apr. 2021.
- [16] X. Wei, Y. Jiang, Q. Liu, and X. Wang, "Calibration of Phase Shifter Network for Hybrid Beamforming in mmWave Massive MIMO Systems," *IEEE Trans. Signal Process.*, vol. 68, pp. 2302–2315, Apr. 2020.
- [17] R. Zhang, B. Shim, and W. Wu, "Direction-of-Arrival Estimation for Large Antenna Arrays With Hybrid Analog and Digital Architectures," *IEEE Trans. Signal Process.*, vol. 70, pp. 72–88, Oct. 2021.
- [18] F. Norouzian, E. Marchetti, M. Gashinova, E. Hoare, C. Constantinou, P. Gardner, and M. Cherniakov, "Rain attenuation at millimeter wave and low-THz frequencies," vol. 68, no. 1, pp. 421–431, 2019.
- [19] E. Björnson, Ö. T. Demir, and L. Sanguinetti, "A primer on near-field beamforming for arrays and reconfigurable intelligent surfaces," in *Asilomar Conference on Signals, Systems, and Computers*, Oct. 2021, pp. 105–112.
- [20] A. M. Elbir, K. V. Mishra, and S. Chatzinotas, "NBA-OMP: Near-field Beam-Split-Aware Orthogonal Matching Pursuit for Wideband THz Channel Estimation," *arXiv*, Feb. 2023.
- [21] X. Wei and L. Dai, "Channel estimation for extremely large-scale massive MIMO: Far-field, near-field, or hybrid-field?" *IEEE Commun. Lett.*, vol. 26, no. 1, pp. 177–181, Nov. 2021.
- [22] M. Cui and L. Dai, "Channel estimation for extremely large-scale MIMO: Far-field or near-field?" *IEEE Trans. Commun.*, vol. 70, no. 4, pp. 2663–2677, Jan. 2022.
- [23] X. Zhang, Z. Wang, H. Zhang, and L. Yang, "Near-field channel estimation for extremely large-scale array communications: A model-based deep learning approach," *IEEE Communications Letters*, vol. 27, no. 4, pp. 1155–1159, 2023.
- [24] W. Lv, K. V. Mishra, and S. Chen, "Co-pulsing FDA radar," *IEEE Transactions on Aerospace and Electronic Systems*, 2022, in press.
- [25] —, "Clutter suppression via space-time-range processing in co-pulsing FDA radar," in *Asilomar Conference on Signals, Systems, and Computers*, 2022, pp. 470–475.
- [26] P. Vouras, K. V. Mishra, A. Artusio-Glimpse, S. Pinilla, A. Xenaki, D. W. Griffith, and K. Egiiazarian, "An overview of advances in signal processing techniques for classical and quantum wideband synthetic apertures," *IEEE Journal of Selected Topics in Signal Processing*, vol. 17, no. 2, pp. 317–369, 2023.
- [27] P. Vouras, K. V. Mishra, and A. Artusio-Glimpse, "Phase retrieval for Rydberg quantum arrays," in *IEEE International Conference on Acoustics, Speech and Signal Processing*, 2023, pp. 1–5.
- [28] R. Schmidt, "Multiple emitter location and signal parameter estimation," *IEEE Trans. Antennas Propag.*, vol. 34, no. 3, pp. 276–280, Mar. 1986.
- [29] X. Yu, G. Cui, J. Yang, L. Kong, and J. Li, "Wideband MIMO radar waveform design," *IEEE Trans. Signal Process.*, vol. 67, no. 13, pp. 3487–3501, 2019.
- [30] M. Cui, L. Dai, Z. Wang, S. Zhou, and N. Ge, "Near-field rainbow: Wideband beam training for XL-MIMO," *IEEE Transactions on Wireless Communications*, vol. 22, no. 6, pp. 3899–3912, Nov. 2023.
- [31] A. M. Elbir, W. Shi, A. K. Papazafireopoulos, P. Kourtessis, and S. Chatzinotas, "Near-field terahertz communications: Model-based and model-free channel estimation," *IEEE Access*, vol. 11, pp. 36 409–36 420, Apr. 2023.
- [32] B. Friedlander and A. J. Weiss, "Direction finding in the presence of mutual coupling," *IEEE Trans. Antennas Propag.*, vol. 39, no. 3, pp. 273–284, Mar. 1991.